Phase Behavior and Miscibility in Two-Component Glycolipid Monolayers

Tetiana Mukhina,* Gerald Brezesinski,* and Emanuel Schneck*

Institute for Condensed Matter Physics, TU Darmstadt, Hochschulstraße 8, 64289 Darmstadt, Germany

E-mail: tetiana.mukhina@pkm.tu-darmstadt.de; gerald.brezesinski@pkm.tu-darmstadt.de; emanuel.schneck@pkm.tu-darmstadt.de

Abstract

Glycolipids are known to be involved in the formation of ordered functional domains in biological membranes. Since the structural characterization of such domains is difficult, most studies have so far dealt with lipid mixtures containing only one glycolipid component at a time, although biological membranes usually contain several glycolipid species, which can result in more complex structures and phase behavior. Here, we combine classical isotherm measurements with surface-sensitive grazing-incidence x-ray diffraction to investigate the phase behavior and miscibility in Langmuir monolayers of binary glycolipid mixtures. We find that the phase behavior has a subtle dependence on the saccharide headgroup chemistry. For compatible chemistries, molecular superlattice structures formed by one of the glycolipid species are conserved and can host foreign glycolipids up to a defined stoichiometry. In contrast, for sterically incompatible saccharide chemistries the superlattice is lost even if both species are able to form such structures in their pure forms. Our results suggest that related phenomena may play important roles also in biological contexts.

Introduction

Biological membranes contain various amounts of glycolipids depending on the membrane type.[1,2] With a great variety of headgroup chemistries, glycolipids exhibit specific interactions with other saccharides[3,4] and proteins[5–7] and can mediate membrane interactions[8,9] and induce membrane adhesion.[10,11] In phospholipid environments, glycolipids are known to promote lipid lateral phase separation,[12–15] which is suited, for instance, to locally condensate membrane proteins[12] or to facilitate vesicle budding.[16] The formation of ordered domains in lipid-based model membranes has been investigated with various experimental and computational methods,[17,18] ranging from fluorescence measurements[19] to x-ray/neutron scattering[20–23] and coarse-grained and atomistic molecular dynamics (MD) simulations.[24,25] Grazing-incidence x-ray diffraction (GIXD)[26] is particularly well suited to study the formation of glycolipid-enriched domains, because the method can identify molecular superlattices which glycolipids in contrast to phospholipids tend to form[27] based on their ability of getting engaged in hydrogen-bond networks (HBNs). We have recently used GIXD to explore the phase behavior of phospholipid/glycolipid mixed monolayers and observed a rich phase behavior ranging from near-complete de-mixing to the formation of mixed ordered domains with unique features, depending on both chain and headgroup chemistry.[23] However, while previous experimental studies on domain formation in model membranes have typically dealt with only one glycolipid component, biological membranes usually contain several glycolipid species at the same time,[1,2] such that the mutual interaction between glycolipids with different headgroups can lead to hitherto unexplored structures and phase behavior of potentially great biological relevance.

In the present study, we use GIXD and isotherm measurements to investigate the structure and phase behavior of Langmuir lipid monolayers containing two types of glycolipids. The distinct diffraction patterns of molecular superlattices reveal interesting new phenomena occuring in these binary mixtures and enable us to construct phase diagrams. When HBNs are compatible, superlattices formed by one of the species are conserved and can host foreign

glycolipids up to a defined stoichiometry. In contrast, when the HBNs are incompatible, the headgroup ordering is lost even if both species are able to form superlattices in their pure forms. As a consequence, subtle differences in the saccharide chemistry can lead to very different behavior. Our results highlight the subtle role of the headgroup chemistry and suggest that phenomena like those observed play important roles also in biological contexts.

Materials and Methods

Materials

Saturated monogalactosyl-diglyceride (MGDG-sat), digalactosyl-diacylglycerol (DGDG-sat), N-hexadecanoyl-ceramide-trihexoside (Trihexo-sat), and N-hexadecanoyl-lactosyl-ceramide (LacCer-sat) were purchased form Matreya Lipids and Biochemicals (State College, Pennsylvania, US). Chloroform (purity $\geq$ 99.9%), methanol (purity $\geq$ 99.9%), and ethanol (purity $\geq$ 99.8%) were purchased from Sigma-Aldrich and used without further purification. Double deionized ultrapure water (resistivity = 18.2 MΩ·cm) was obtained from a Milli-Q purification station. Solutions of glycolipid/glycolipid mixtures were prepared by dissolving lipid powder at concentrations of 1 mg/mL in a mixture of chloroform, methanol, and water (2:1:0.1 by volume).

Pressure-area isotherm measurements

Pressure-area isotherms were collected at 20°C at the Langmuir trough (R&K, Potsdam, Germany) at the P08 beamline at DESY or at an in-house Langmuir trough (Accurion, KSV NIMA, Biolin Scientific, Espoo, Finland), both equipped with a Wilhelmy paper plate pressure sensor. The lipid solution was spread onto the air/water interface using a Hamilton syringe. After solvent evaporation ($\approx$ 15 min) the formed monolayers were compressed to the target lateral pressure with a compression speed of $\mathrm{d}A^{\mathrm{a}}_{\mathrm{lip}}/\mathrm{d}t \approx$ 2-5 Å^2/min, where $A^{\mathrm{a}}_{\mathrm{lip}}$ is the available area per molecule. The pressure data were collected with an estimated pressure

accuracy of $\pm$ 0.1 mN/m and with an estimated accuracy of $\pm$ 0.5 Å^2 in $A_{\mathrm{lip}}^{\mathrm{a}}$ after calibration.

GIXD

Grazing-incidence x-ray diffraction (GIXD) experiments were carried out at the beamline P08 at storage ring PETRA III of Deutsches Elektronen-Synchrotron (DESY, Hamburg, Germany) with the same setup described in a previous study,[23] from which the following description is largely reproduced.

The incident beam of 15 keV energy (wavelength $\lambda = 0.826$ Å) strikes the air/water interface at a grazing angle of $\alpha_{\mathrm{i}} = 0.07°$, below the critical angle α_{cr} of total external reflection ($\alpha_{\mathrm{i}} = 0.85{\cdot}\alpha_{\mathrm{cr}}$), such that only the immediate vicinity of the interface is probed with an evanescent wave with a decay length of $\approx$ 80 Å. The beam footprint on the water surface was 1 mm x 60 mm. The Langmuir trough was enclosed in a helium-filled sealed container with Kapton windows for the x-ray beam. The subphase temperature was maintained at 20°C with a water flow thermostat, and monitored during measurements. A ground glass plate was placed in the beam footprint $\approx$ 1 mm below the water surface in order to damp the vibration of the water surface and thus to enhance the quality of the diffraction signals. The diffraction signal was collected with a one-dimensional position sensitive detector (PSD, Mythen2 1K, PSI, Villigen, Switzerland) by scanning the azimuth angle 2θ and, with that, the in-plane component $Q_{xy} = (4\pi/\lambda)\sin(\theta)$ of the scattering vector $\boldsymbol{Q} = (Q_{xy}, Q_z)^{\mathrm{T}}$. The out-of-plane component,$Q_z = (2\pi/\lambda)\left[\sin(\alpha) + \sin(\alpha_{\mathrm{i}})\right]$, is encoded in the vertical position of the PSD channels, where α denotes the angle between the scattered direction and the sample plane. The in-plane beam divergence was collimated with a Soller collimator placed in front of the PSD providing $\Delta_{2\theta} \approx 0.09°$ (full-width-at-half-maximum, FWHM), corresponding to $w_{xy}^{\mathrm{res}} = (4\pi/\lambda)\sin(\Delta_{2\theta}/2) \approx 0.012$ Å^{-1}.

A representative example of an experimental $I(Q_{xy}, Q_z)$ map (linear color scale) and the modeled intensity are shown in Fig. 1 A and B. The integrated intensities in Q_{xy}- and Q_z-directions are shown in panels C and D, respectively. To reconstruct the 2D crystalline

structure of the monolayers, the diffraction peaks on the resulting intensity maps $I(Q_{xy}, Q_z)$ were analyzed as described previously.[23,28] In brief, the Q_{xy} and Q_z positions and widths of the peaks were obtained in a least-square fitting procedure and the lattice and superlattice parameters (units cell dimensions, in-plane area per chain A_{xy}, cross-sectional area per chain A_0, chain tilt angle t, among others) were then reconstructed from the peak positions as described before.[23,27,29] Finally, the average areas of the ordered domains were obtained from the peak widths as detailed in.[23]

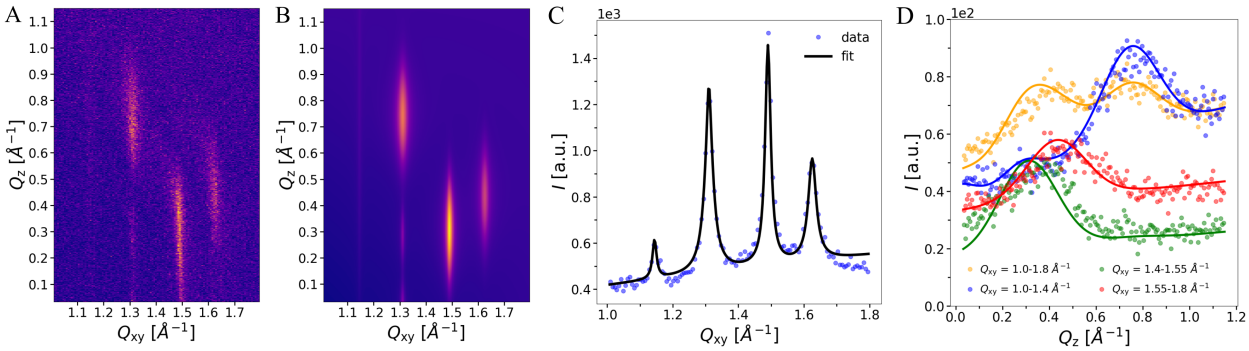

Figure 1: (A) GIXD pattern (intensity vs. Q_{xy} and Q_z) of an equimolar MGDG-sat/DGDG-sat mixed monolayer at $\pi = 30$ mN/m. (B) Modeled intensity. (C) Q_z–integrated intensity vs. Q_{xy}. (D) Piece-wise Q_{xy}–integrated intensity vs. Q_z, where the integration ranges are given in the legend. For clarity, the total intensity (yellow data points and curve) was divided by a factor of 2.

Results and Discussion

Fig. 2 shows the chemical structures of the glycolipids investigated. Mono- and digalactosyldiglyceride (MGDG and DGDG, comprising one or two galactose units, respectively) are the main constituents of the thylakoid membranes of chloroplasts,[2] while lactosylceramide with a lactose headgroup (LacCer) and ceramide-trihexoside with a (galactose)-(galactose)-(glucose) headgroup (Trihexo) have numerous functional roles in signal transduction.[30,31] In the following, we will refer to these molecules as MGDG-sat, DGDG-sat, LacCer-sat, and Trihexo-sat, where the suffix "sat" is used to indicate that the variants investigated comprise predominantly saturated hydrocarbon chains.[10] We will first recapitulate the behavior of

the glycolipids in single-component monolayers and subsequently present results on binary glycolipid mixtures at various mixing ratios.

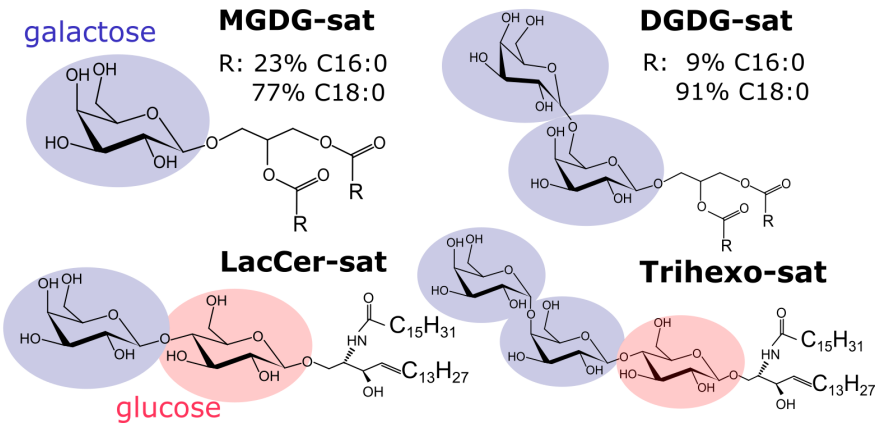

Figure 2: Chemical structures of the glycolipids MGDG-sat, DGDG-sat, LacCer-sat, and Trihexo-sat.

Single-component glycolipid monolayers

As reported earlier,[27] DGDG-sat and Trihexo-sat at sufficiently high lateral pressures form chain-ordered structures without molecular superlattice, termed liquid-condensed (LC) phase in the following. In contrast, MGDG-sat and LacCer-sat form highly ordered structures with superlattices (termed SL in the following) comprising two and four molecules, respectively, as shown in the Supporting Information (Section S1 and S4, Tables S1-S3, S8-S10). The SL is stabilized by a hydrogen-bond network (HBN) between the sugar headgroups.[23,27] Fig. 3 A shows the compression and decompression isotherms of single-component monolayers of all glycolipids investigated. The available area per lipid, $A_{\mathrm{lip}}^{\mathrm{a}}$, as measured with the Langmuir trough, was calibrated by setting it equal to the crystallographic area per lipid, $A_{\mathrm{lip}}^{\mathrm{c}}$, as determined by GIXD at high lateral pressure (here: $\pi = 30$ mN/m). This procedure is valid whenever the monolayer assumes only one single phase. The isotherm of MGDG-sat is characterised by a sharp pressure increase at low areas ($A_{\mathrm{lip}}^{\mathrm{a}} \lesssim 50$ Å^2), suggesting that ordered SL domains are formed immediately upon spreading.[23] These domains are initially ill-defined (depending on the solvent and the spreading procedure) and coexist with a two-dimensional

gaseous phase of individual molecules. The first monolayer compression has an annealing effect, which is why the decompression isotherm is even steeper and can be considered as a better representative of thermal equilibrium. The isotherm of LacCer-sat (see Fig. 3 A) is overall less steep and the difference between first compression and decompression is even more pronounced. A small kink on the decompression isotherm at $\pi \approx 9$ mN/m can be noticed, however it is so weak that we refrain from any further analysis or interpretation. For DGDG-sat, which does not form SL domains, the difference between compression and decompression is minimal. However, we notice a larger difference ($\approx 10\%$) between $A_{\mathrm{lip}}^{\mathrm{c}}$ and $A_{\mathrm{lip}}^{\mathrm{a}}$ in the low-pressure region. Even if the data sheet states a high percentage of C18 chains, the fatty acid composition of hydrogenated natural lipids might still contain shorter chain lengths due to different growth conditions. Such 'impurities' will clearly contribute to the area in the isotherm and the monolayer compressibility but not to the scattering intensity. The compression isotherm of Trihexo-sat monolayer clearly exhibits a transition plateau from a liquid expanded (LE) to the LC phase, which is less pronounced upon decompression, likely because the slow transition kinetics would require much lower compression/decompression speeds.

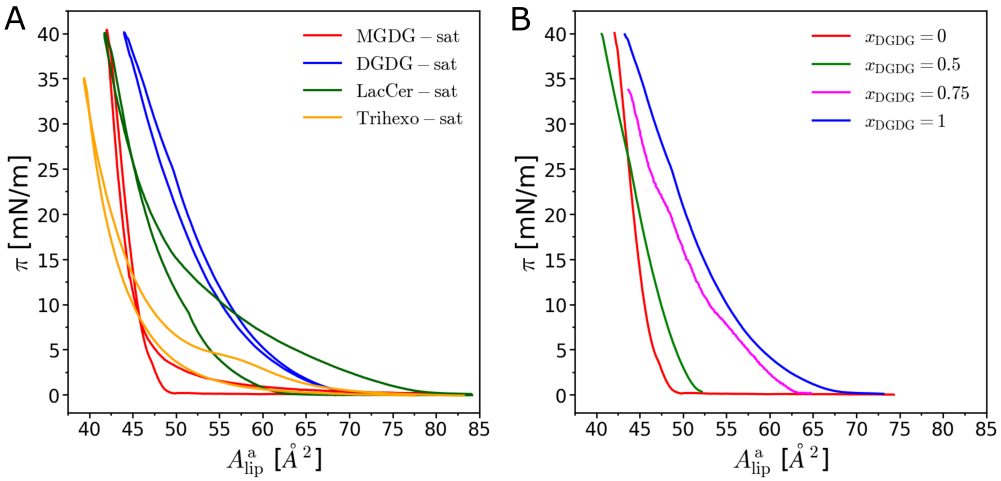

Figure 3: (A) Isotherms of the glycolipids MGDG-sat, DGDG-sat, LacCer-sat, and Trihexo-sat. (B) Isotherms of MGDG-sat/DGDG-sat mixed monolayers (DGDG-sat mole fraction x_{DGDG}) together with those of the pure components ($x_{\mathrm{DGDG}} = 0$ and $x_{\mathrm{DGDG}} = 1$). The available area per lipid $A^{\mathrm{a}}_{\mathrm{lip}}$ was calibrated with the crystallographic area per lipid $A^{\mathrm{c}}_{\mathrm{lip}}$ in the LC or SL phase at $\pi = 30$ mN/m in all cases. The values for $A^{\mathrm{c}}_{\mathrm{lip}}$ of MGDG-sat, LacCer-sat, and Trihexo-sat were taken from reference.[27] For $x_{\mathrm{DGDG}} = 0.75$, a more complicated calibration was used, see main text.

Binary glycolipid monolayers

We move on to discuss the behavior of binary glycolipid mixtures with at least one glycolipid type capable of forming an SL phase on its own. To this end, we have investigated MGDG-sat monolayers containing either DGDG-sat, LacCer-sat, or Trihexo-sat at defined mole fractions x.

MGDG-sat mixed with DGDG-sat: host/guest superlattice formation

Fig. 3 B shows crystallographically calibrated isotherms of MGDG-sat/DGDG-sat mixtures with various DGDG-sat mole fractions x_{DGDG}, including pure MGDG-sat ($x_{\mathrm{DGDG}} = 0$) and pure DGDG-sat ($x_{\mathrm{DGDG}} = 1$). We recall that pure MGDG-sat forms a rigid SL phase at all lateral pressures, leading to a very steep isotherm, while pure DGDG-sat forms a more deformable LC phase coinciding with a more gradual pressure increase.[27] A first important observation is that the isotherm of the equimolar MGDG-sat/DGDG-sat mixture

($x_{\mathrm{DGDG}} = 0.5$) is steep and looks much like the one of pure MGDG-sat.

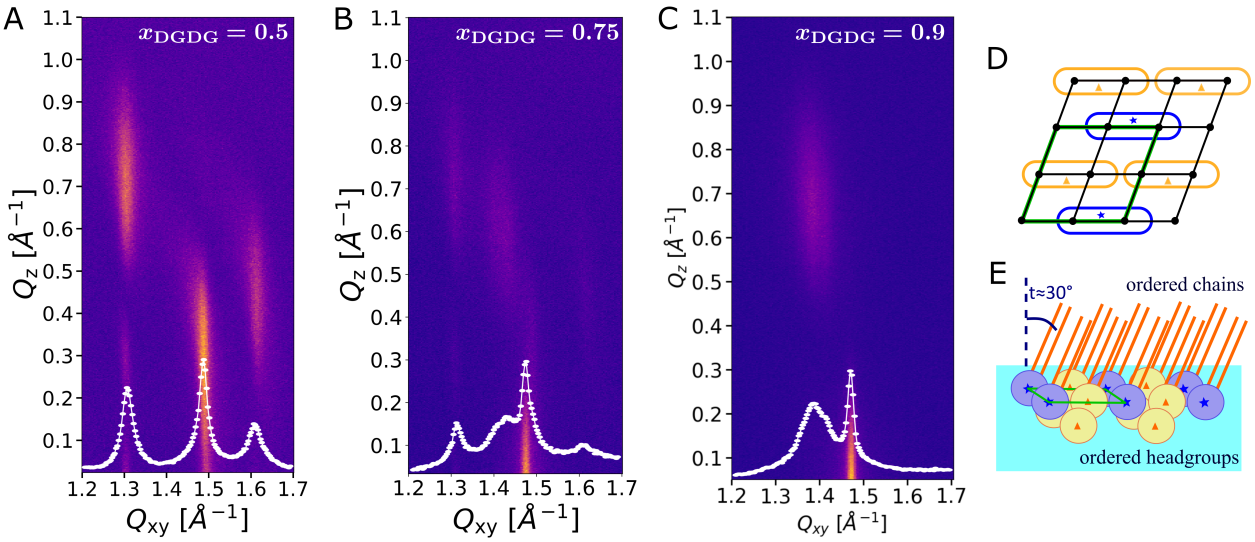

Figure 4: (A–C) GIXD patterns of MGDG-sat/DGDG-sat mixed monolayers at $\pi = 30$ mN/m for $x_{\mathrm{DGDG}} = 0.5$ (A), $x_{\mathrm{DGDG}} = 0.75$ (B), and $x_{\mathrm{DGDG}} = 0.9$ (C). (D) Schematic top-view representation of one of the possible structures of the observed superlattice in the equimolar MGDG-sat/DGDG-sat mixture. Black dots, blue stars, and orange triangles indicate the positions of the chains and of the MDGD-sat and DGDG-sat headgroups, respectively. Black lines indicate the repeating unit cell of the alkyl chains. The repeating unit cell of the molecular superlattice is indicated with a green parallelogram. Blue and orange ellipsoids represent the delimitation of MGDG-sat and DGDG-sat molecules, respectively. (E) A schematic side-view representation of the same structure.

Fig. 4 A shows the GIXD pattern of this mixture at $\pi = 30$ mN/m. Strikingly, the diffraction pattern and the associated lattice parameters are almost identical to those obtained for the SL of pure MGDG-sat, and there is no indication of any other coexisting phase. Minor differences in the structural parameters with respect to pure MGDG-sat concern the chain tilt t, which decreases from $t = 32°$ at $x_{\mathrm{DGDG}} = 0$ to $t = 30°$ at $x_{\mathrm{DGDG}} = 0.5$, and the crystallographic area per lipid, which decreases from 43.3 Å^2 to 42.8 Å^2. The remarkable similarity between these structures implies that the superlattice comprises one MGDG-sat molecule and one DGDG-sat molecule in a supercell that closely resembles that of pure MGDG-sat (see Fig. 4 D and E for a schematic illustration). Obviously the distal galactose unit of DGDG-sat can be accommodated underneath the HBN of the proximal galactose units without disturbing the packing properties up to the equimolar mixture. The incor-

poration of additional DGDG-sat molecules into this superlattice appears to be sterically impossible, such that phase separation has to occur. According to this interpretation, a diffraction pattern like the one described should only be observed up to $x_{\mathrm{DGDG}} = 0.5$ but not at higher DGDG-sat contents.

In order to test this hypothesis, a monolayer with $x_{\mathrm{DGDG}} = 0.75$ was investigated. Its isotherm (see Fig. 3 B) differs considerably from that of the equimolar mixture and features considerable compressibility, similar to pure DGDG-sat, but with a significant change in the slope at $\pi \approx 8$ mN/m. Fig. 4 B shows the GIXD pattern at $\pi = 30$ mN/m, which appears complex at first glance but which can readily be described as a superposition of the SL diffraction pattern at $x_{\mathrm{DGDG}} = 0.5$ (with virtually identical parameters) and the diffraction pattern of an oblique LC phase that resembles that of pure DGDG-sat. With $A^{\mathrm{c}}_{\mathrm{lip}} = 44.2$ Å^2 and $t = 27°$, this LC phase is however slightly more upright and densely packed than that of pure DGDG-sat ($A^{\mathrm{c}}_{\mathrm{lip}} = 46.8$ Å^2 and $t = 32°$, see Supporting Information, Table S5). In summary, these observations support the above hypothesis of a 50 mol% capacity of the MGDG-sat SL phase for DGDG-sat molecules. At $x_{\mathrm{DGDG}} = 0.75$, to good approximation 50 mol% of all lipids are thus in the SL phase, while the other 50 mol% of all lipids (almost exlusively DGDG-sat) are in the LC phase. This notion was in fact used to crystallographically calibrate the isotherm of the MGDG-sat/DGDG-sat mixture at $x_{\mathrm{DGDG}} = 0.75$ (Fig. 3 B), where we assumed $A^{\mathrm{a}}_{\mathrm{lip}} = A^{\mathrm{c}}_{\mathrm{lip}}(\mathrm{SL})/2 + A^{\mathrm{c}}_{\mathrm{lip}}(\mathrm{LC})/2$.

Fig. 4 C shows the GIXD pattern at $x_{\mathrm{DGDG}} = 0.9$, featuring the diffraction peaks associated with a single LC phase, as observed for pure DGDG-sat, and without any sign of phase separation. In other words, the SL phase vanishes above a certain value of x_{DGDG}. The structural parameters of the LC phase observed at $x_{\mathrm{DGDG}} = 0.9$ ($A^{\mathrm{c}}_{\mathrm{lip}} = 45.6$ Å^2 and $t = 30°$) are intermediate between those at $x_{\mathrm{DGDG}} = 0.75$ and $x_{\mathrm{DGDG}} = 1$ (see above), reflecting that an increase in the MGDG-sat fraction systematically enhances the lipid packing in the LC phase due to the favorable sterical interactions.

GIXD on mixtures with $x_{\mathrm{DGDG}} \leq 0.5$ shows that the SL phase exists already at low pres-

sure (measurement performed at $\pi = 4$ mN/m) and persists up to high pressures. For $x_{\mathrm{DGDG}} = 0.75$, the SL phase emerges only above intermediate pressures (measurement performed at $\pi = 12$ mN/m), while at low pressure ($\pi = 2$ mN/m) only the LC phase was detected. This behavior is consistent with the change in compressibility at $\pi \approx 8$ mN/m observed in the corresponding isotherm. For the mixture with $x_{\mathrm{DGDG}} = 0.9$, no SL phase was observed up to $\pi = 30$ mN/m.

The obtained results enable us to construct the phase diagram of MGDG-sat in mixture with DGDG-sat (Fig. 5). We recall that only up to one DGDG-sat molecule per MGDG-sat molecule can be integrated into the SL domains, while the excess amount of DGDG-sat present at higher x_{DGDG} is excluded and forms a coexisting DGDG-sat-enriched LC phase that significantly differs from pure DGDG-sat. This scenario (SL+LC) corresponds to a miscibility gap in the phase diagram. Further increasing x_{DGDG} leads to the relative growth of the LC phase at the cost of the SL phase until the SL phase vanishes at a threshold value of x_{DGDG}, which increases with the lateral pressure. For higher DGDG-sat contents, only the LC phase is left. For instance at $\pi = 30$ mN/m, $x_{\mathrm{DGDG}} = 0.75$ is still in the miscibility gap, while $x_{\mathrm{DGDG}} = 0.9$ is already located in the monophasic LC region of the phase diagram.

As seen from the crystallographic parameters obtained under different conditions, the tightest molecular packing is achieved at $x_{\mathrm{DGDG}} = 0.5$, indicating overall favorable sterical interactions between MGDG-sat and DGDG-sat. The free energy gain associated with the formation of the highly ordered SL structure of MGDG-sat based on an HBN must be strong since, according to the phase diagram, much less MGDG-sat can be incorporated into the LC phase of DGDG-sat than DGDG-sat molecules can be incorporated into the SL phase of MGDG-sat.

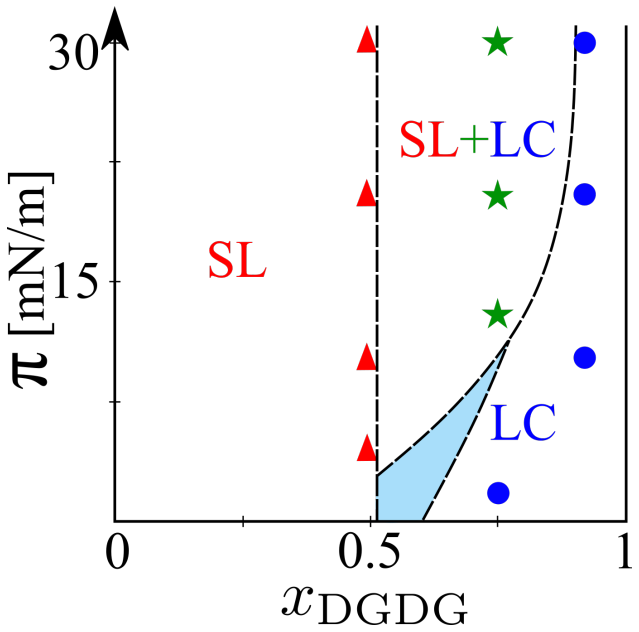

Figure 5: Phase diagrams of MGDG-sat in mixtures with DGDG-sat. Triangles, circles, and stars indicate the points where the GIXD measurements revealed SL phases, LC phases, or SL+LC phase coexistence, respectively. The precise course of the boundary between CL and the miscibility gap region (SL + LC) remains uncertain due to an insufficient number of data points. The light blue region schematically indicates this uncertainty.

The widths of the diffraction peaks in Q_{xy}-direction encode the average sizes A_{d} of the ordered domains (see Methods section). Fig. 6 presents A_{d} at $\pi = 30$ mN/m for various MGDG-sat/DGDG-sat mixed monolayers. The values are summarized in Table S28 in the Supporting Information. The domain sizes are of the order of 200–400 nm^2 and no significant differences between SL and LC phases were observed. This is in contrast to our earlier results on phospholipid/glycolipid mixtures,[23] where the domains were generally larger in the LC phases (with comparatively low glycolipid contents), which has been attributed to a greater ability of structurally more adaptable LC phases to anneal defects. The fact that no such trend is observed for binary glycolipid mixtures in the present study indicates that glycolipids may generally be less efficient at defect annealing than phospholipids, possibly because the dynamics of glycolipid headgroups is dominated by comparatively long-lived hydrogen bonds also in LC phases.

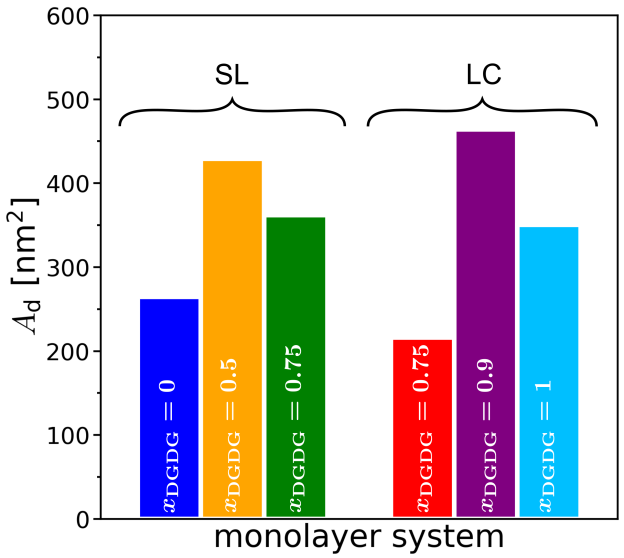

Figure 6: Average sizes A_d of the ordered domains for MGDG-sat, DGDG-sat and their mixtures at $\pi = 30$ mN/m. Data for pure MGDG-sat were taken from Ref.[27]

MGDG-sat mixed with LacCer-sat or Trihexo-sat: loss of superlattice

Fig. 7 A shows the isotherms of equimolar mixtures of MGDG-sat with LacCer-sat ($x_{\text{LacCer}} = 0.5$) and Trihexo-sat ($x_{\text{Trihexo}} = 0.5$) along with the isotherms of the pure components. The isotherms are steep and do not indicate any phase transition. Fig. 7 B shows the GIXD pattern of a MGDG-sat/Trihexo-sat mixed monolayer at $x_{\text{Trihexo}} = 0.5$ and $\pi = 30$ mN/m. The diffraction peaks reveal a single LC phase with an rectangular lattice of tilted chains with $t = 20.4°$ and $A^c_{lip} = 43.0$ Å^2. As shown in Fig. S17 in the Supporting Information, t decreases gradually with increasing pressure. We recall that lipids with Trihexo headgroup, in contrast to MGDG-sat, do not to form any SL phase on their own.[23,27] Instead, an LC phase with $t = 12°$ and $A^c_{lip} = 40.2$ Å^2 was reported at $\pi = 30$ mN/m (see Table S7 in the Supporting Information). The absence of a molecular superlattice in the mixture indicates that the two components do mix but the characteristic HBN that stabilizes the SL phase of pure MGDG-sat is incompatible with the chemical structure of the Trihexo-sat headgroup. Since SL formation is observed in equimolar MGDG-sat mixtures with DGDG-sat, the incompatibility must be attributed to the chemical moieties that are different in Trihexo-sat,

notably the inner glucose moiety and the ceramide linkage. Apparently, the free-energy reduction that would be associated with a superlattice formation is less pronounced and over-compensated by the mixing entropy. A more favorable packing can be ruled out as the driving force because the crystalline area per lipid in the mixed LC phase, $A^{c}_{lip} = 43.0$ Å^2, is slightly larger than what would result from ideal mixing, $[A^{c}_{lip}$(MGDG-sat)$+A^{c}_{lip}$(Trihexo-sat)$]/2 = 41.8$ Å^2.

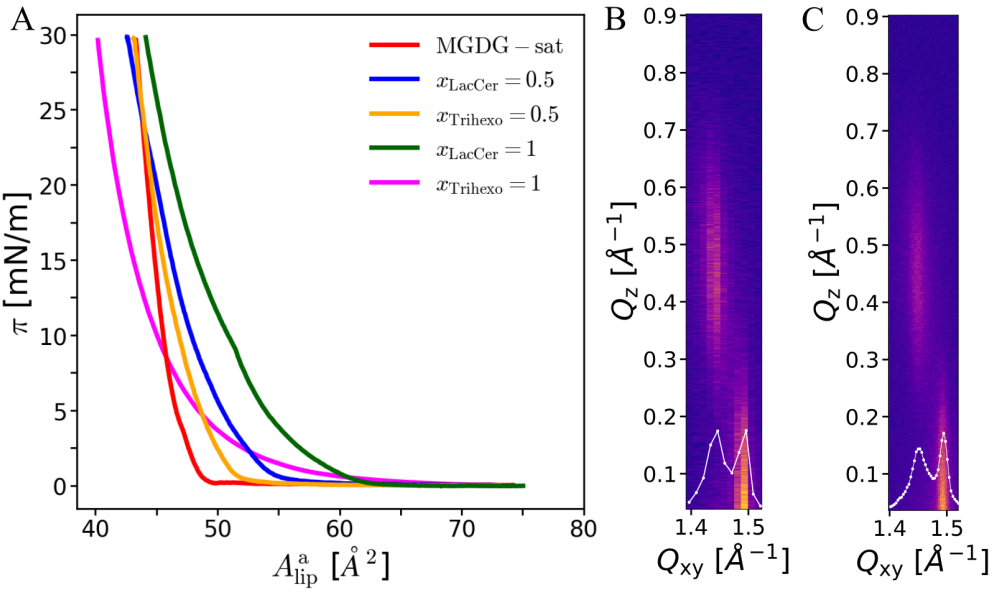

Figure 7: (A) Isotherms of equimolar MGDG-sat/LacCer-sat and MGDG-sat/Trihexo-sat mixed monolayers together with those of the pure components. (B and C) GIXD patterns of equimolar MGDG-sat/Trihexo-sat (B) and MGDG-sat/LacCer-sat (C) mixed monolayers, both at $\pi = 30$ mN/m.

A similar mixed LC structure, albeit oblique rather than rectangular, is observed for MGDG-sat/LacCer-sat monolayers at $x_{LacCer} = 0.5$ and $\pi = 30$ mN/m, for which the GIXD pattern is shown in Fig. 7 C. The absence of a molecular superlattice is remarkable because both lipid components were reported to form SL phases in their pure forms.[23,27] The crystalline area per lipid in the mixed LC phase at $\pi = 30$ mN/m, $A^{c}_{lip} = 42.6$ Å^2, is slightly smaller than what would result from ideal mixing, $[A^{c}_{lip}$(MGDG-sat)$+A^{c}_{lip}$(LacCer-sat$)]/2 = 43.7$ Å^2 suggesting more favorable sterical interactions between the non-like sugar headgroups.

To probe the miscibility range we have investigated MGDG-sat/LacCer-sat mixed monolayers with LacCer-sat mole fractions $x_{\mathrm{LacCer}} = 0.25$ and 0.75 (see Supporting Information, Section S11 and S12 for the GIXD data and structural parameters). Single mixed rectangular and oblique LC phases were observed for $x_{\mathrm{LacCer}} = 0.25$ and 0.75 molar compositions, respectively. However, a closer look at the diffraction pattern for $x_{\mathrm{LacCer}} = 0.75$ reveals the existence of two additional weak intensity peaks at $Q_{xy} \approx 1.42$ Å^{-1} and $Q_{xy} \approx 1.63$ Å^{-1}, likely originating from the crystalline structure of phase-separated LacCer-sat molecules. In the following we will use for this phase the generic term "C", as motivated further below. The associated Q_{xy} positions are alike to the ones of the pure LacCer-sat monolayer[27] (see Fig. S3 in Section S5 in Supporting Information). Therefore, the observation of these extra-peaks suggests that the mixture with $x_{\mathrm{LacCer}} = 0.75$ lies in a miscibility gap between an LacCer-sat-enriched C phase and an LC phase with similar contents of MGDG-sat and LacCer-sat. Since the sample with $x_{\mathrm{LacCer}} = 0.5$ forms a single homogeneous LC phase, one border of the miscibility gap must thus be located between $x_{\mathrm{LacCer}} = 0.5$ and $x_{\mathrm{LacCer}} = 0.75$. The proposed phase diagram for MGDG-sat/LacCer-sat is shown in Fig. 8.

The crystalline area per lipid $A^{\mathrm{c}}_{\mathrm{lip}} = 42.4$ Å^2 in the LC phase at $x_{\mathrm{LacCer}} = 0.75$ is very similar to the one at $x_{\mathrm{LacCer}} = 0.5$ ($A^{\mathrm{c}}_{\mathrm{lip}} = 42.6$ Å^2). But when starting from pure MGDG-sat ($x_{\mathrm{LacCer}} = 0$), the addition of a small LacCer-sat fraction ($x_{\mathrm{LacCer}} = 0.25$, where a single LC phase is observed, too) leads to a considerable decrease in $A^{\mathrm{c}}_{\mathrm{lip}}$, from 43.3 Å^2 to 41.6 Å^2, indicating that packing is optimal for comparatively low values of x_{LacCer}. Following this reasoning, the sterically favorable formation of the mixed LC phase, together with the mixing entropy, free-energetically outperforms superlattice formation.

Coming back to the phase diagram in Fig. 8, SL/LC phase coexistence has to emerge below a certain value of x_{LacCer} because, according to the so-called miscibility selection rule of liquid crystals,[32,33] complete miscibility in a two-component system requires that the two components alone exhibit the same phase type.[23] Moreover, a single SL phase has to be recovered for very low x_{LacCer} and, similarly, for x_{LacCer} approaching 1, the LC has to vanish

and single C phase must appear. Most importantly however, in a wide range of x_{LacCer}, mixing of MGDG-sat and LacCer-sat leads to a complete loss of the headgroup ordering although both glycolipids assume headgroup-ordered SL structures in their pure forms. This behavior is in strong contrast to the formation of a molecular superlattice in the equimolar mixture when LacCer-sat is replaced with DGDG-sat, which has a disaccharide headgroup, too (see above). The discrepancy demonstrates once again the high sensitivity of the phase behavior to subtle chemical details.

At this point it should be noted that the phase diagram in Fig. 8 was constructed based on data obtained with LacCer-sat with two different alkyl chain lengths. While LacCer-sat with C18 chains was used for monolayers with $x_{\mathrm{LacCer}} = 0.25$ and $x_{\mathrm{LacCer}} = 0.75$, LacCer-sat with C16 chains was used for pure LacCer-sat monolayers in reference[27] and for monolayers with $x_{\mathrm{LacCer}} = 0.5$ in the present work. However, our previous results on MGDG-sat in mixtures with phospholipid have shown that the phase diagrams obtained with C16 and C18 phospholipids are qualitatively identical,[23] suggesting that the same applies to MGDG-sat/LacCer-sat mixtures. GIXD experiments with pure C18-LacCer-sat (Fig. S3, Section S5 in the Supporting Information) revealed two Debye-Scherrer rings at $Q_{xy} \approx 1.42$ Å^{-1} and $Q_{xy} \approx 1.62$ Å^{-1} at all lateral pressures, originating from surface-adsorbed 3D crystallites, termed "Cr" phase in the following. For pure C16-LacCer-sat, an SL phase was observed at all pressures, while Debye-Scherrer rings only emerged at high lateral pressures ($\pi = 30$ mN/m).[27] Apparently the slightly stronger van der Waals interactions between the chains of C18-LacCer-sat promote crystallite formation more strongly. Based on the notion of different types of crystalline phases of LacCer-sat, whose prevalence at given conditions depends on the chain length, we use in the phase diagram (Fig 8) the generic term "C" which refers to both SL and Cr phases.

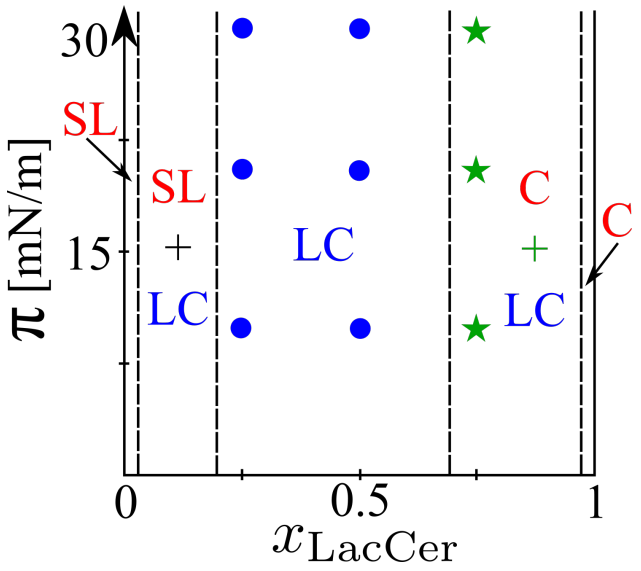

Figure 8: Phase diagram of MGDG-sat in mixtures with LacCer-sat. Circles and stars indicate the points where the GIXD measurements revealed LC phases or C+LC phase coexistence, respectively. The label "C" is used to indicate either an SL phase or a bulk-crystalline Cr phase.

Conclusions

The phase and miscibility behavior of binary glycolipid mixtures in monolayers at the air/water interface was studied by GIXD and isotherm measurements. First, we investigated mixtures of MGDG-sat, which has a monogalactose headgroup and forms a molecular superlattice (SL) in its pure form, with DGDG-sat, which has a digalactose headgroup and is unable to form an SL due to steric hindrance. Interestingly, for DGDG-sat mole fractions below 50%, the SL of MGDG-sat is able to host virtually all DGDG-sat molecules, because steric hindrance does not occur as long as there is only up to one DGDG-sat molecule per di-molecular unit cell. The SL structure preferred by MGDG-sat is conserved because the proximal galactose unit of DGDG-sat is compatible with the hydrogen-bond network (HBN) that stabilizes the SL. Further addition of DGDG-sat leads to phase separation into an SL phase that is saturated with DGDG-sat (equimolar mixture) and an LC phase, rich in DGDG-sat, that is less ordered. The LC phase of DGDG-sat can accommodate only a small

fraction of MGDG-sat molecules ($\approx$ 15 mol%). The SL persists up to a very high DGDG-sat fraction. In contrast, as observed for mixtures of MGDG-sat with Trihexo-sat or LacCer-sat, which have a different headgroup linker and the proximal monosaccharide is a glucose, the incompatibility of hydrogen-bond donor and acceptor geometries can disrupt the HBN and thus suppress formation of a mixed SL phase, even if both mixed glycolipid components exhibit SL phases in their pure forms.

Although the lipids investigated here, because of their fully saturated tails, have an unusually strong tendency to form ordered structures, the phenomena and mechanisms described here likely play considerable roles also in biological contexts because biomembranes are known to typically exist close to phase boundaries with ordered states.[34,35]

Further insights may be gained in the future by investigating ternary and multicomponent lipid mixtures containing glycolipids. In mixtures of two glycolipid species with a phospholipid, for instance, competition may occur between the formation of a joint SL (as observed here) and the formation of less ordered phospholipid/glycolipid mixed phases (as observed in our previous study[23]). Complementary atom-scale insights into the HBNs of SL phases may be gained with the help of molecular dynamics simulations. However, correctly reproducing the observed SL unit cells is currently still a challenge because of long equilibration times compared to those of LC phases or equivalent L_{β}' bilayer phases which are nowadays routinely studied in simulations.[36,37]

Acknowledgement

We acknowledge DESY (Hamburg, Germany), a member of the Helmholtz Association HGF, for the provision of experimental facilities. Parts of this research were carried out at PETRA III and we would like to thank Chen Shen, René Kirchhof, and Milena Lippmann for assistance during the beamtime at P08 and chemistry lab, respectively. Beamtime was allocated for proposal(s) I-20190719, I-20191281, I-20200672, and I-20210377. Financial support by

the German Research Foundation (DFG) via Emmy-Noether grant SCHN 1396/1 and via grant SCHN 1396/2 is gratefully acknowledged. We thank Irina Berndt, Fabio Strati, Julio Pusterla, and Laura Mortara for help with sample preparation and measurements.

Supporting Information Available

Experimental and simulated GIXD patterns and parameter tables; table domain sizes.

References

(1) Van Meer, G.; Voelker, D. R.; Feigenson, G. W. Membrane lipids: Where they are and how they behave. *Nature reviews Molecular cell biology* **2008**, *9*, 112–124.

(2) Boudière, L.; Michaud, M.; Petroutsos, D.; Rébeillé, F.; Falconet, D.; Bastien, O.; Roy, S.; Finazzi, G.; Rolland, N.; Jouhet, J.; et al. Glycerolipids in photosynthesis: composition, synthesis and trafficking. *Biochimica et Biophysica Acta (BBA)-Bioenergetics* **2014**, *1837*, 470–480.

(3) Bucior, I.; Burger, M. M. Carbohydrate–carbohydrate interactions in cell recognition. *Current Opinion in Structural Biology* **2004**, *14*, 631–637.

(4) Spillmann, D.; Burger, M. M. Carbohydrate-carbohydrate interactions in adhesion. *Journal of Cellular Biochemistry* **1996**, *61*, 562–568.

(5) Lis, H.; Sharon, N. Lectins: Carbohydrate-specific proteins that mediate cellular recognition. *Chemical Reviews* **1998**, *98*, 637–674.

(6) Zanetta, J.-P.; Kuchler, S.; Lehmann, S.; Badache, A.; Maschke, S.; Thomas, D.; Dufourcq, P.; Vincendon, G. Glycoproteins and lectins in cell adhesion and cell recognition processes. *The Histochemical Journal* **1992**, *24*, 791–804.

(7) Sharon, N.; Lis, H. Lectins as cell recognition molecules. *Science* **1989**, *246*, 227–234.

(8) Yu, Z.; Calvert, T.; Leckband, D. Molecular forces between membranes displaying neutral glycosphingolipids: Evidence for carbohydrate attraction. *Biochemistry* **1998**, *37*, 1540–1550.

(9) Kanduč, M.; Schlaich, A.; de Vries, A. H.; Jouhet, J.; Maréchal, E.; Demé, B.; Netz, R. R.; Schneck, E. Tight cohesion between glycolipid membranes results from balanced water–headgroup interactions. *Nature communications* **2017**, *8*, 1–9.

(10) Latza, V. M.; Demé, B.; Schneck, E. Membrane adhesion via glycolipids occurs for abundant saccharide chemistries. *Biophysical Journal* **2020**, *118*, 1602–1611.

(11) Kav, B.; Demé, B.; Gege, C.; Tanaka, M.; Schneck, E.; Weikl, T. R. Interplay of trans-and cis-interactions of glycolipids in membrane adhesion. *Frontiers in molecular biosciences* **2021**, *8*, 754654.

(12) Brown, D. A.; Rose, J. K. Sorting of GPI-anchored proteins to glycolipid-enriched membrane subdomains during transport to the apical cell surface. *Cell* **1992**, *68*, 533–544.

(13) Fra, A. M.; Williamson, E.; Simons, K.; Parton, R. G. Detergent-insoluble glycolipid microdomains in lymphocytes in the absence of caveolae. *Journal of Biological Chemistry* **1994**, *269*, 30745–30748.

(14) Kopitz, J. Lipid glycosylation: A primer for histochemists and cell biologists. *Histochemistry and cell biology* **2017**, *147*, 175–198.

(15) Watkins, E. B.; Frey, S. L.; Chi, E. Y.; Cao, K. D.; Pacuszka, T.; Majewski, J.; Lee, K. Y. C. Enhanced ordering in monolayers containing glycosphingolipids: Impact of carbohydrate structure. *Biophysical journal* **2018**, *114*, 1103–1115.

(16) Nguyen, D. H.; Hildreth, J. E. Evidence for budding of human immunodeficiency virus type 1 selectively from glycolipid-enriched membrane lipid rafts. *Journal of virology* **2000**, *74*, 3264–3272.

(17) Marquardt, D.; Heberle, F. A.; Nickels, J. D.; Pabst, G.; Katsaras, J. On scattered waves and lipid domains: Detecting membrane rafts with X-rays and neutrons. *Soft Matter* **2015**, *11*, 9055–9072.

(18) Sezgin, E.; Levental, I.; Mayor, S.; Eggeling, C. The mystery of membrane organization: composition, regulation and roles of lipid rafts. *Nature reviews Molecular cell biology* **2017**, *18*, 361–374.

(19) Jacobson, K.; Mouritsen, O. G.; Anderson, R. G. Lipid rafts: At a crossroad between cell biology and physics. *Nature cell biology* **2007**, *9*, 7–14.

(20) Frey, S. L.; Chi, E. Y.; Arratia, C.; Majewski, J.; Kjaer, K.; Lee, K. Y. C. Condensing and fluidizing effects of ganglioside GM1 on phospholipid films. *Biophysical Journal* **2008**, *94*, 3047–3064.

(21) Armstrong, C. L.; Barrett, M.; Toppozini, L.; Kučerka, N.; Yamani, Z.; Katsaras, J.; Fragneto, G.; Rheinstädter, M. C. Co-existence of gel and fluid lipid domains in single-component phospholipid membranes. *Soft Matter* **2012**, *8*, 4687–4694.

(22) Armstrong, C. L.; Marquardt, D.; Dies, H.; Kučerka, N.; Yamani, Z.; Harroun, T. A.; Katsaras, J.; Shi, A.-C.; Rheinstädter, M. C. The observation of highly ordered domains in membranes with cholesterol. *PLoS One* **2013**, *8*, e66162.

(23) Mukhina, T.; Brezesinski, G.; Shen, C.; Schneck, E. Phase behavior and miscibility in lipid monolayers containing glycolipids. *Journal of Colloid and Interface Science* **2022**, *615*, 786–796.

(24) Manna, M.; Róg, T.; Vattulainen, I. The challenges of understanding glycolipid functions: An open outlook based on molecular simulations. *Biochimica et Biophysica Acta (BBA)-Molecular and Cell Biology of Lipids* **2014**, *1841*, 1130–1145.

(25) Pantelopulos, G. A.; Nagai, T.; Bandara, A.; Panahi, A.; Straub, J. E. Critical size dependence of domain formation observed in coarse-grained simulations of bilayers composed of ternary lipid mixtures. *The Journal of Chemical Physics* **2017**, *147*, 095101.

(26) Als-Nielsen, J.; Jacquemain, D.; Kjaer, K.; Leveiller, F.; Lahav, M.; Leiserowitz, L. Principles and applications of grazing incidence X-ray and neutron scattering from ordered molecular monolayers at the air-water interface. *Physics Reports* **1994**, *246*, 251–313.

(27) Stefaniu, C.; Latza, V. M.; Gutowski, O.; Fontaine, P.; Brezesinski, G.; Schneck, E. Headgroup-ordered monolayers of uncharged glycolipids exhibit selective interactions with ions. *The Journal of Physical Chemistry Letters* **2019**, *10*, 1684–1690.

(28) Jensen, T. R.; Kjaer, K. Structural properties and interactions of thin films at the air-liquid interface explored by synchrotron X-ray scattering. *Novel methods to study interfacial layers* **2001**, *11*, 2054.

(29) Kjaer, K.; Als-Nielsen, J.; Helm, C. A.; Tippman-Krayer, P.; Moehwald, H. Synchrotron x-ray diffraction and reflection studies of arachidic acid monolayers at the air-water interface. *The Journal of Physical Chemistry* **1989**, *93*, 3200–3206.

(30) Sonnino, S.; Prinetti, A.; Nakayama, H.; Yangida, M.; Ogawa, H.; Iwabuchi, K. Role of very long fatty acid-containing glycosphingolipids in membrane organization and cell signaling: The model of lactosylceramide in neutrophils. *Glycoconjugate journal* **2009**, *26*, 615–621.

(31) Ashkenazi, S.; Cleary, T. G. Rapid method to detect Shiga toxin and Shiga-like toxin

I based on binding to globotriosyl ceramide (Gb3), their natural receptor. *Journal of clinical microbiology* **1989**, *27*, 1145–1150.

(32) Sackmann, H.; Demus, D. The problems of polymorphism in liquid crystals. *Molecular Crystals and Liquid Crystals* **1973**, *21*, 239–273.

(33) Sackmann, H. Thermodynamic aspects of polymorphism in liquid crystals. *Pure and Applied Chemistry* **1974**, *38*, 505–527.

(34) Hänel, F.; Brezesinski, G.; Hilliger, M.; Gräfe, U.; Dörfler, H.-D. Thermal regulation of phospholipid fluidity in Corynebacterium glutamicum. *Journal of basic microbiology* **1986**, *26*, 409–413.

(35) Mužić, T.; Tounsi, F.; Madsen, S. B.; Pollakowski, D.; Konrad, M.; Heimburg, T. Melting transitions in biomembranes. *Biochimica et Biophysica Acta (BBA)-Biomembranes* **2019**, *1861*, 183026.

(36) Jambeck, J. P.; Lyubartsev, A. P. Derivation and systematic validation of a refined all-atom force field for phosphatidylcholine lipids. *The journal of physical chemistry B* **2012**, *116*, 3164–3179.

(37) Kowalik, B.; Schubert, T.; Wada, H.; Tanaka, M.; Netz, R. R.; Schneck, E. Combination of MD simulations with two-state kinetic rate modeling elucidates the chain melting transition of phospholipid bilayers for different hydration levels. *The Journal of Physical Chemistry B* **2015**, *119*, 14157–14167.

TOC Graphic

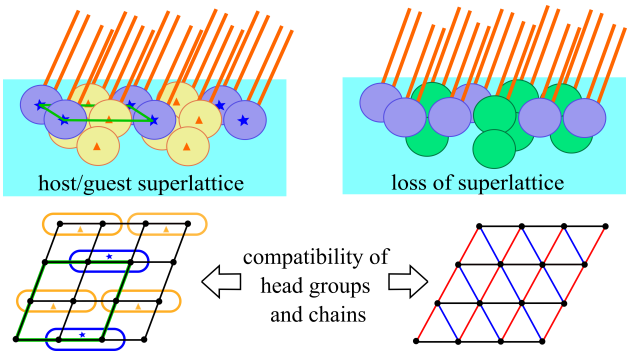

Figure : TOC Graphic.